1	
2	A Comparative Study of Automated Infrasound Detectors - PMCC and AFD with Analyst
3	Review
4	
5	Junghyun Park*, Chris T. Hayward, Cleat P. Zeiler, Stephen J. Arrowsmith, and Brian W. Stump
6	
7	*Corresponding author
8	Roy M. Huffington Department of Earth Sciences
9	Southern Methodist University
10	3225 Daniel Avenue
11	Dallas, TX 75205, USA
12	(pjh2521920@gmail.com)
13	
14	
15	
16	
17	
18	
19	
20	
21	
22	
23	

24 Abstract

25

26

27

28

29

30

31

32

33

34

35

36

37

38

39

40

41

42

43

44

45

Automated detections calculated by the progressive multi-channel correlation (PMCC) method (Cansi, 1995) and the adaptive F detector (AFD) (Arrowsmith et al., 2009) are compared to the signals identified by five independent analysts. Each detector was applied to a four-hour time sequence recorded by the Korean infrasound array CHNAR. This array was used because it is composed of both small (<100 m) and large (~1000 m) aperture element spacing. The fourhour time sequence contained a number of easily identified signals under noise conditions that have average RMS amplitudes varied from 1.2 to 4.5 mPa (1 to 5 Hz), estimated with running five-minute window. The effectiveness of the detectors was estimated for the small aperture, large aperture, small aperture combined with the large aperture, and full array. The full and combined arrays performed the best for AFD under all noise conditions while the large aperture array had the poorest performance for both detectors. PMCC produced similar results as AFD under the lower noise conditions, but did not produce as dramatic an increase in detections using the full and combined arrays. Both automated detectors and the analysts produced a decrease in detections under the higher noise conditions. Comparing the detection probabilities with Estimated Receiver Operating Characteristic (EROC) curves we found that the smaller value of consistency for PMCC and the larger p-value for AFD had the highest detection probability. These parameters produced greater changes in detection probability than estimates of the falsealarm rate. The detection probability was impacted the most by noise level, with low noise (average RMS amplitude of 1.7 mPa) having an average detection probability of ~40% and high noise (average RMS amplitude of 2.9 mPa) average detection probability of ~23%.

46

### 48 Introduction

Renewed interest in infrasound has been stimulated by the use of acoustic gauges in the International Monitoring System (IMS), which ultimately will be comprised of 60 infrasonic arrays to monitor nuclear testing (Christie and Campus, 2010). Additionally, about 100 infrasound arrays operate continuously worldwide (Hedlin *et al.*, 2012). The density of infrasound stations combines to increasing and in some areas now includes regional coverage, i.e. USArray Transportable Array (Veron *et al.*, 2012). Near-surface sources such as earthquakes, volcanic eruptions and mining explosions generate both seismic and infrasonic signals (Hagerty *et al.*, 1999) and so both seismic and infrasound studies can contribute to source identification. Moreover, an automated system for infrasound detection will reduce analyst workloads in analyzing large data sets and thus streamline detection process, the first step towards source location and ultimately source characterization.

In response to the need to identify in excess of 1,000 events per month at a single array (Evers and Haak, 2001; Matoza *et al.*, 2013) several automated infrasound detectors have been developed including the progressive multi-channel correlation (PMCC) algorithm (Cansi, 1995), the standard F-detector (Blandford, 1974) incorporated in Infra Tool (Hart, 2004) and the adaptive F detector (AFD) (Arrowsmith *et al.*, 2009) incorporated in InfraMonitor. Since regional and global signals are strongly influenced by time-varying propagation effects, each detector uses a waveform correlation technique applied to array data, rather than a high-fidelity template matching approach. Based on the assumption that noise is uncorrelated, PMCC applies progressive processing to the data recorded by different sensors in an array by first assessing cross-correlation functions of sub-arrays and then adding additional array elements in order to

reduce false alarms (Cansi, 1995). The method estimates trace velocities and azimuths from subarrays and then progressively increases the network aperture. Infra Tool calculates an azimuth, trace velocity, correlation coefficient, and a conventional F-statistic (Blandford, 1974; 2002) for each time segment using multiple overlapping windows that move through the data volume. This detector performs well in cases with high values of correlation and an associated high F-statistic (Garcés and Hetzer, 2002). AFD (Arrowsmith *et al.*, 2009) modifies the conventional F-statistic based on a time-varying empirical estimate of the background noise, producing a time-adaptive F-statistic. Brown *et al.* (2008) utilizes the Hough transform (Hough, 1959) for the automatic detection of acoustic signals based on the premise that static sources will have a constant azimuth over time in the case of the low signal-to-noise ratio (SNR). An important criteria in this work, similar to detection of seismic phases (Zeiler and Velasco, 2009), is the association of multiple detections to estimate the event location.

Detection methods can be evaluated in terms of their Receiver Operating Characteristic (ROC) curve (Kay, 1998) that quantifies the relationship between the probability of detection and the probability of false alarm as a function of the detector threshold. The challenge of ROC curve analyses lies in developing a realistic labeled dataset for which the signals are known and span the space of possible signal characteristics, while the noise spans the space of possible noise characteristics. An effort to develop such a dataset for regional and global infrasound monitoring is currently underway at Commissariat à l'Energie Atomique (CEA), Los Alamos National Laboratory (LANL), Southern Methodist University (SMU), and Korea Institute of Geoscience and Mineral Resources (KIGAM), and at the International Data Centre (IDC). This approach to develop a pseudo-synthetic dataset using real signals and noise can be thought of as a compromise between purely synthetic datasets (the standard for ROC curve analyses), in which

there is total control over the labels (signals and noise), and purely real datasets in which the labels are not truly known and must be estimated by analysts. This paper focuses on the estimation of ROC curves using real data and an analyst approach, and motivates the more comprehensive study being undertaken by the consortium of institutions mentioned above. In order to assess the performance of automated detectors, a series of tests using analysts' review of the same data were undertaken as has been done in similar seismic observation studies. Freedman (1966) first studied estimates of picking errors from analyst reviewed seismograms using nine analysts and researchers. Sereno (1990) and Leonard (2000) assessed automatic picks comparing results with those produced by analysts and quantified the misclassification of seismic phases, mis-timing of seismic phases, and poor phase association (Sipkin *et al.*, 2000). Zeiler and Velasco (2009) focused on measurements by highly experienced analysts at a number of institutions. They concluded that the main contributing factors to pick errors for analyst are ambient noise levels, distance from source to receiver, magnitude, source mechanisms, and propagation effects.

We compare two automated infrasound detectors to a manually reviewed time sequence of data and provide a testing procedure based on a limited data set. The test procedure for PMCC and AFD was to apply varying detection parameters to the same data set, a four-hour sequence of infrasound data at the Korean infrasound array, CHNAR. This array was selected because it has both a short (< 100 m) and long (~1000 m) aperture spacing. The four-hour time sequence was chosen due to the number of easily identified signals as well as a transition from low to high wind noise conditions half way through the time period. The results of the automated procedures are compared to picks by five independent analysts of varying experience as a step towards assessing the effectiveness of these procedures in terms of changing environmental conditions

during the time period of the dataset. In order to assess the detection performance, we determine the *Estimated* Receiver Operator Curves (*E*ROC) rather than the more traditional approach. However, in the absence of true data with ground truth (referred to above as 'labeled' data), it is important to provide a protocol in order to compare detectors and one possible way is to synthesize signals that are as realistic as possible in a future assessment. Arrowsmith *et al.* (2008) performed synthetic tests in multi-array detection, association, and location of infrasound in order to assess network location resolution.

125 Detectors

*AFD* 

In the presence of time varying background noise, AFD (Arrowsmith *et al.*, 2009) incorporated in InfraMonitor uses the F-statistic with the null hypothesis of perfectly uncorrelated noise as suggested by Blandford (2002). Automatic detection is based on the F-statistic calculated as the power on the beam from the array divided by the average over all channels of the power of the difference between the beam and the individual array channels:

133 
$$F = \left(\frac{J-1}{J}\right) \frac{\sum_{n=n_0}^{n_0+(N-1)} \left[\sum_{j=1}^{J} x_j(n+l_j)\right]^2}{\sum_{n=n_0}^{n_0+(N-1)} \left(\sum_{j=1}^{J} \left\{x_j(n+l_j) - \left[\frac{1}{J}\sum_{m=1}^{J} x_m(n+l_m)\right]\right\}^2\right)},$$
 (1)

where J is the number of sensors,  $x_j(n)$  is the waveform amplitude of the nth sample of the meanfree time series from sensor j,  $l_j$  is the time-alignment lag obtained from beamforming,  $n_0$  is the starting sample index for the processing interval, and N is the number of samples in the processing window. The F-statistic is implemented using the maximum average cross correlation for beam formation, and associated p-value, which is the probability of obtaining a F-statistics at least as extreme as the calculated values under F-distribution:  $p\{F(t)\}$ , from all elements in an array for each time window.

In the presence of correlated noise, the theoretical F-statistic is distributed as:

$$CF_{2BT,2BT(N-1)} \tag{2}$$

where B is the bandwidth of the filtered data and T is the length of the processing (detection) window over which the power is averaged, N is the number of array elements, and C is given by:

$$C = \left(1 + N \frac{P_s}{P_n}\right) \tag{3}$$

where Ps/Pn denotes the signal-to-noise ratio (Shumway *et al.*, 1999), referring to the ratio of the correlated-noise power to uncorrelated-noise power ratio (Arrowsmith *et al.*, 2008). The constant, C, is the scaling factor that aligns the peak of the distribution of the F-statistic in the time window with the peak of the theoretical central F-distribution with 2BT, 2BT(N-1) degrees of freedom. This constant is proportional to the number of sensors and the correlated-noise to uncorrelated-noise ratio, and becomes 1 when the correlated-noise power Ps=0.

The standard F detector can be modified so that it is adaptive in time, capturing change in noise characteristics with estimates of C for subsequent adaptive windows when the total time window duration is larger than adaptive window. The observed distribution of the F-statistic  $(F_{2BT,2BT(N-1)})$ , computed from the output of a standard frequency-wavenumber (F-K) analysis (e.g. Rost & Thomas, 2002) and original input parameters, is adapted to the computed F-distribution  $(CF_{2BT,2BT(N-1)})$  by estimating the maximum C-value which aligns the peaks of the two distributions. The remapped F-statistic is converted to a *p*-value so a standard *p*-value threshold can be used to declare a detection with a specified statistical significance. Processing parameters used for the detection tests are summarized in Table 1. In these tests, *p*-values of 0.01 and 0.05

were used. The estimation of these parameters and their relationship to environmental conditions that change as a function of time are discussed by Park (2013).

PMCC

The PMCC algorithm (Cansi, 1995) assumes uncorrelated noise, resulting in false alarms in the presence of correlated noise. It is based on progressive processing data recorded by subarrays from a larger array using time domain cross-correlation estimates between individual stations (Cansi, 1995). The first step in PMCC uses cross-correlation to measure the time delay  $\Delta t_{ij}$  between all pairs of signals,  $S_i(t)$  and  $S_j(t)$  at station i and j, in each three-element subarray. In the case of a wave propagating without distortion, the delay is the same for all frequencies in the contributing signal (Cansi and Le Pichon, 2009):

$$\Delta t_{ij} = \frac{1}{2\pi f} (\varphi_j(f) - \varphi_i(f)), \qquad (4)$$

where  $\varphi_i(f)$  and  $\varphi_j(f)$  represent the phase at station i and j. For a plane wave signal observed at three sensors, the sum of time delays from these stations obeys a closure relation, which is used as a phase detector:

$$\Delta t_{ij} + \Delta t_{jk} + \Delta t_{ki} = 0, \tag{5}$$

The second PMCC step is progressive (Cansi and Le Pichon, 2009) where the consistency of the set of delays is estimated with all the sensors (n) of a sub-network, $R_n$ , and is defined as the mean quadratic residual of the closure relations (Cansi and Le Pichon, 2009):

180 
$$R_n \ni i, j, k \begin{cases} r_{ijk} = \Delta t_{ij} + \Delta t_{jk} + \Delta t_{ki} \\ C_n = \sqrt{\frac{6}{n(n-1)(n-2)}} \sum_{i>j>k} r_{ijk}^2. \end{cases}$$
 (6)

When the consistency,  $C_n$ , is below a threshold, a detection is declared on  $R_n$ . The network aperture is progressively increased in order to provide the most robust estimates of signal phase velocity and azimuth. Hereafter, to avoid a confusion of consistency  $(C_n)$  with C-value of Equation (3), we will call it the consistency value.

Garcés and Hetzer (2002) investigated the utility of PMCC to detect various infrasound signals including microbaroms, surf noise, volcanic arrivals, as well as signals from bolides, aircraft, and spacecraft, observed in Hawaii. Campus and Christie (2010) assessed the detection of various natural infrasound sources such as earthquakes, the calving of icebergs and glaciers, and volcanic eruptions as well as man-made sources such as a rocket launch and mining activities. These studies illustrate that parameters for optimum PMCC processing depend on infrasonic signal characteristics, array configuration, and background noise.

Detector testing focuses on regional infrasound arrays with signals from 1 to 5 Hz associated with natural and man-made events. Initial PMCC tuning parameters were set based on the work of Garcés and Hetzer (2002) as well as experience with AFD documented in the next section of this paper. Detection parameters used for the initial test are summarized in Table 1. Threshold consistency values (defined as the maximum consistency threshold for declaring a detection) of 0.1 and 0.5 s were used. One advantage of PMCC is that the detections are assessed in both the time and frequency domain. Each frequency band within each time window represents a "pixel" of data, which is analyzed independently, followed by comparison of adjacent pixels in time and frequency, where nearest-neighbor "pixels" with similar characteristics are classified as "families" (Garcés and Hetzer, 2002).

A standard deviation of  $10^{\circ}$  for azimuth and 20 m/s for phase velocity with a phase velocity range from 0.2 to 0.5 km/s were used in grouping the families. The distribution of

backazimuths as well as phase velocities may be seasonal variable and depend on the specific infrasonic arrival but in this initial study these effects were not considered. Incorporation of this type of information might require some type of iterative procedure linked to phase identification as well as the analysis of a broader set of data covering much larger time periods.

### Data and Analysis

A four-hour-dataset (02:00:00-06:00:00 in UTC, 11am-3pm in local time, Julian day 002, 2012) recorded by the seismo-acoustic array, CHNAR is used in this analysis. The array consists of a small infrasound array with an approximate 100 m aperture embedded in a larger approximate 1 km aperture array (Figure 1) with a second or sub-infrasound element approximately 50 m from the gauge in the larger array. There are a total of 11 microbarometers (Chaparral Physics Model 2.0 microphones) and 4 seismometers (GS-13). Data is sampled at 40 sample/s. The center of the array has a weather station measuring wind velocity, wind azimuth, and temperature, installed 2 m above the surface, sampled at 1 sample/s. Each microbarometer is attached to ten porous hoses, each eight meters in length connected at the center in a star-like configuration for reducing background noise generated by wind along the turbulent boundary layer. Data is recorded on 24-bit digitizers (Geotech DR24) and sent in real time via radio telemetry to KIGAM in South Korea and forwarded to SMU in Texas.

PMCC and AFD were both applied to this dataset. The four-hour dataset has noise levels that increase after the first two hours producing two data segments with different background noise levels. The first two hours of data were recorded under wind conditions near 0 m/s, while wind velocity increased in the second two hours to an average of 3 m/s. Filtered (1-5 Hz)

waveforms are shown in Figure 2, with four easily identified large signals near 03:00:00 UTC along with the initial output from PMCC discussed latter.

The two detectors were tested using four different starting configurations or sub-networks summarized in Table 2. As mentioned earlier, one difference between PMCC and AFD is the use of sub-networks. In the small and large aperture array tests AFD and PMCC used the same array configuration. However, when the small and large aperture arrays were combined, AFD used all array elements together, while PMCC applies two sub-networks, one small and one large aperture. Since each sub-network has a total of four elements, the threshold of 4 sensors was used. The PMCC estimates involve two steps, the first calculates the detection parameters from the small aperture array and then reevaluates adding the large aperture array elements. The second step estimates the detection parameters from the large aperture array and then reevaluates adding the small aperture array elements. These two estimates are combined to produce the final parameters for a total of three sub-networks (Table 2).

AFD remaps the F-distribution in time to account for time varying noise conditions using the C value (Equation (3)). Figure 3 documents the change in this value with time for the complete data set. C values for the different array configurations tested are displayed and compared to five-minute averages of wind velocity and azimuth at the site. A one-hour adaptive window was used during the InfraMonitor processing based on the detector tuning study of Park, 2013. Estimates based on all array apertures for the first two-hours of data have relatively high C values (1.5-2.7) associated with low wind velocities from the north and east, while the last two-hours of data have smaller C values of 1.1 to 1.8, with higher wind velocities and azimuths from the northwest (Figure 3). Waveforms after 04:00:00 UTC have significantly higher background noise than those before (Figure 2). In the large aperture tests, the C values are not as variable in

time as for the small aperture tests which may reflect decreased correlation of signals under low noise conditions for the large aperture array consistent with local noise sources. Generally, the variation of C value is larger for the smaller array aperture. In all cases C is dependent on weather conditions, especially wind speed. It is not possible to make a definitive conclusion about the relationship between C and wind conditions because of the small time window analyzed in this study. However, this result is consistent with the tuning study (Park *et al.*, 2011) where the C-value decreased with increasing wind velocity and documented in the study by Park (2013).

Automatic detections are dependent on background noise levels as well as algorithmic tuning parameters and so sensitivity tests for both detectors were conducted with respect to different values of consistency for PMCC, 0.1 and 0.5 s, and p-value, 0.01 and 0.05, for AFD. Larger consistency values for PMCC provide the ability to include a greater number of automated detections at expense of the quality of the signals across the array. The use of a larger p-value in AFD includes a greater number of detections that depart from the null hypothesis, and may include correlated noise. Results for a wider range of consistency and p-value are presented later.

An example detection output from PMCC with a consistency of 0.1 s using all arrays is given in Figure 4, showing the number of sensors, consistency, correlation, amplitude, azimuth, and phase velocity for each identified signal. Detections with small consistency values using all array elements in the final calculation were observed during the first two hours of data, while few detections under the consistency constraints were found in the last two hours of data when the background noise levels were higher.

The sensitivity tests for the two detectors using all array configurations - PMCC (S), PMCC (L), PMCC (S+L), PMCC (All), AFD (S), AFD (L), AFD (S+L), and AFD (All) - are summarized in Figure 5 (see the Table 2 for configuration information). Tests with consistency values of 0.1 and 0.5 s for PMCC are designated PMCC.1s and PMCC.5s and those with *p*-values of 0.01 and 0.05 for AFD are designated AFD.01 and AFD.05. The number of detections in each case are summarized in Table 3 with histograms comparing them in Figure 6. The automatic detections using the larger values of consistency, 0.5 s, and *p*-value, 0.05, included all the automated detections using the lower values of consistency, 0.1 s, and *p*-value, 0.01.

Both automatic detectors produce a larger number of detections using either the combined small and large aperture arrays or all array elements compared to the cases where only the large aperture array was used. In some cases, detections using both the small and large aperture arrays appear to combine individual detections found using the small and large aperture arrays separately. The number of detections estimated by AFD is almost two times greater than the number estimated by PMCC with many of the additional detections from AFD occurring in the last two-hour time period when the wind noise increases (Figure 5). The number of detections increases significantly when the consistency for PMCC and the *p*-value for AFD are increased. The largest increase in detections occurs with the high *p*-value for AFD. The strong signals around 03:00:00 UTC were detected with high correlation and consistent phase velocities of 300-400 m/s by both detectors. The azimuth distributions for the detections are primarily from the southeast with a secondary set of detections from the northwest (Figure 5, right).

## **Analyst Review**

Five analysts reviewed the four-hour dataset. The results of the analysts review are used to assess the automated detectors. Each person was free to define unique criteria for event identification (Table 4). The experience levels of the analysts were variable, three labeled as experts based on a long history of signal analysis and two as new and undergoing training. All used time domain and f-k based tools in Geotool (Coyne and Henson, 1995) to identify signals. The numbers of detections produced by the five analysts are compared to the output of the automatic detectors in Figure 6. The detection numbers by all analysts are significantly higher than those determined by either automated detector. AFD and PMCC each used a 20 s time window with 50 % overlap and therefore multiple phases within the time window can only be separately identified by the analysts. The frequency band of filtering applied by each analyst also varied slightly based on individual interpretations of the data.

In most cases, the picks by the analysts included all the events identified by the two automatic detectors (Figure 7). In the case of the last two hours of data, where the noise levels are higher, there are fewer automated detections and a reduced number of detections identified by the analysts. This result highlights that detection under higher background noise conditions is difficult for both automatic systems and humans.

The azimuth and phase velocity estimates for the signals are summarized in Figure 8. A large portion of the identified signals come from azimuths clustered around 150° and 300° before 04:00:00 UTC, the time period with low background noise levels. It is difficult to distinguish between automatic and analysts' detections since both sets of estimates overlap for this time period. In the case of AFD.05, there are consistent detections from 240° for all aperture arrays in the full dataset which might be generated from local noise with a high F-statistics. The azimuth estimates for signals in the second two-hour time period are more scattered. Phase velocities

range from 320 to 350 m/s with a similar distribution of values produced by automatic and human estimates. Polar plots of phase velocity further documents the changing distribution of detections over the four-hour time period with detections distributed from 90° to 180° and from 270° to 330° for the first two hours (Figure 9). The source of these clusters may be local signals associated with human activities. In the last two hours of data, the automatic and human detections are more scattered although in the case of human detections there is a cluster from approximately 300° to 330°. This implies that either infrasound signals from 90° to 180° stopped or were masked by the noise after the first two hours or the environmental conditions are such that propagation to the station is impeded.

### Estimated Receiver Operating Characteristic Curves

In order to assess detector performance, Receiver Operating Characteristic (ROC) curves can be used to quantify the detection and false alarm probabilities (Johnson and Dudgeon, 1993), providing a basis for detector optimization. This approach has been used to quantify the performance of adaptive and conventional detectors of AFD as noted by Arrowsmith *et al.* (2009). ROC curves estimate the trade-off between the detection probability ( $P_D$ ) and the false-alarm probability ( $P_F$ ) for a range of detection thresholds as defined by:

$$P_D = \frac{\text{Number of detected signals}}{\text{Total number of signals}},$$
 (7)

$$P_F = \frac{\text{Number of noise detections}}{\text{Total number of detection intervals during noise}}.$$
 (8)

ROC analysis can be accomplished by inserting known signals of varying size into realistic noise in order to provide a known number of signals within a data set. As an alternative,

we introduce a modified data centric procedure that compares the results of the automated detectors against the detections identified by analysts. The total number of signals is defined by the analyst results in this application and is therefore an alternative performance assessment in the absence of ground truth. In order to distinguish this approach with others, we call these curves *Estimated* Receiver Operator Curves (*E*ROC) to distinguish them from the more traditional approach.

There may be an implicit difference in the duration of the detected signals identified by the automatic detectors and the human analysts since each uses different criteria for picking arrival times. For example, analysts were free to make several arrival picks in a 20-second window, the processing time used by both automatic detectors. In order to reduce this effect, the 4-hour data set was evenly divided into consecutive 20-second window, each window evaluated for detections. Based on Equations (7) and (8), a total of 720 tests were conducted in order to estimate detection and false alarm probability based on the review of all the analysts.

The EROC analysis is subdivided into the first two-hours of data (Figure 10) and the last two-hours of data (Figure 11) as result of the changing noise conditions. Depending on the reference values (analysts) used in estimating the EROC, the curves change. For example if the analyst identifies a smaller number of signals it is possible that the EROC will move towards an ideal detector. A broader range of p-values (0.01 to 0.09) and consistency values (0.1 s to 0.9 s) were used in these comparisons in order to more fully explore the detection space.

During the first two-hours of data, the two automated detectors using all array elements or small and large aperture arrays together have higher detection probabilities than when they just use the small or large aperture arrays alone (Figure 10). PMCC produces a higher detection probability (0.40-0.78) than AFD (0.22-0.45). It also produces a more limited range of lower

false alarm probabilities (0.03-0.07) than AFD (0.01-0.11). In the case of PMCC, tests using a consistency of 0.5 (PMCC.5s) had higher detection probabilities while the false-alarm probabilities increases slightly. Detection probability estimates using PMCC were only slightly affected by changes in the dimension of the initial aperture with some small increase in detection probability using large aperture arrays. PMCC detections using the smaller consistency value produced higher detection probabilities in this analysis, up to 0.78 in the case of Analyst 2. The detection probabilities produced by AFD increased using the higher *p*-value under low noise conditions. However, the false alarm rate also increased, especially for the cases where the small aperture array were used. This result implies that AFD detects more signals identified by the analysts at the expense of more false events.

Under high noise conditions, both automatic detectors produce low detection probabilities with a maximum detection probability of 0.45, compared to 0.78 under low noise conditions. The detection probabilities for both PMCC and AFD cover similar ranges, 0 to 0.45 (Figure 11). PMCC has slightly higher detection and false-alarm probabilities when compared to Analyst 1. Since PMCC produced few detections (conservative detection) in this time period, the false-alarm rate is the same using any of analysts for comparison. On average detection probabilities for AFD are higher for the larger *p*-values. The advantage of using a moving window to correct for time variations in background noise are illustrated when noise condition change with time. During the high noise conditions, analysts reported difficulty in identifying signals with the possibility that a number of signals might have gone undetected or that some of the detections represented coherent noise across the array. The dependence of the *E*ROC results on the analysts illustrates an intrinsic difficulty in this empirical assessment procedure.

In order to assess the impact of increasing wind velocity on the detection process, the average RMS amplitude and average wind velocity during 5 minute windows for the complete data set were estimated. First, the waveforms were filtered in the frequency band of 1 to 5 Hz. The average RMS amplitude,  $AA_{RMS}$ , with respect to time was calculated using waveforms from all array elements as defined:

$$AA_{RMS} = \sqrt{\frac{\sum_{i=1}^{T} \left( \left( \sum_{j=1}^{N} A^{2} \right) / N \right)}{\Delta T}}, \tag{9}$$

where A is the amplitude of waveform at a particular sample, N is the number of infrasound array elements, T is the time window, and  $\Delta T$  is the total time duration. These estimates are plotted in Figure 12 and document the strong correlation between RMS amplitude and wind velocity during this four-hour time period. The average five-minute RMS noise amplitudes varied from 1.2 to 4.5 mPa in the frequency band of 1 to 5 Hz. The amplitude and duration of the detected signals by Analyst 5 are also displayed in Figure 12, illustrating that relatively small amplitude signals were detected under low noise condition, while the number of small amplitude detections are greatly reduced during the higher background noise. In summary, the detection probability was most affected by noise level, with low noise conditions (average amplitude of 1.7 mPa) having an average detection probability of ~40% and high noise conditions (average amplitude of 2.9 mPa) producing an average detection probability of ~23%.

Using these same five-minute windows, the number of detections produced by the automatic detectors and the analysts were counted and compared against the RMS amplitude and wind speed (Figure 13). Generally, the numbers of automatic and human detections are dependent on the RMS amplitude which is correlated with wind velocity. When the small

aperture arrays were used by AFD in both AFD.01 and AFD.05, a significantly higher number of detections were identified during higher average RMS amplitudes.

The number of analyst's detections in all cases increases for average RMS amplitudes between 1.2 and 3.2 mPa, and includes most all the signals detected by the automated procedures (Figure 14(a)). Most analysts identified signals under higher noise conditions although the largest number of detections identified by the analysts was identified during noise conditions with average RMS amplitudes below 3.2 mPa. In the case of AFD.01 and AFD.05, a number of detections were identified under higher RMS noise conditions. Figure 14(b) shows the relationship between the SNR and the number of detections for both the automatic and manual detectors with the step rise in number of detections that occurs for values above 45.

#### Conclusions and Discussion

This study provides an initial investigation of two detectors, AFD and PMCC, using a four-hour time sequence (02:00:00-06:00:00 in UTC, 11am-3pm in local time, Julian day 002, 2012) at CHNAR located within the continent in South Korea. This time period had approximately two hours of low wind velocity and noise and two hours of increased wind and noise. The array consists of a large (~1 km) and small (< 100 m) aperture providing a variety of spatial scale lengths for detecting signals and separating noise. Automatic detections are dependent on tuning parameters specific to each procedure and background noise level. A number of tuning parameters are common to the two approaches and are dependent on the character of the signals including the length of 20 s, overlap of 50%, and filtered band from 1 to 5 Hz based on the regional infrasonic signals. In the case of PMCC, the standard deviation of 10°

for azimuth and 20 m/s for phase velocity with a phase velocity range from 0.20 to 0.5 km/s were used for grouping into families. For AFD, the adaptive window of 1 hour was used and the range of phase velocity and azimuth were unconstrained. Sensitivity tests for both detectors were conducted with respect to different values of consistency (0.1s to 0.9 s) for PMCC and p-value (0.01 to 0.09) for AFD.

Azimuth and phase velocity estimates for the signals identified by both automatic detectors and human analysts are consistent before 04:00:00 UTC (low noise conditions), while the estimates are scattered after 04:00:00 UTC (high noise conditions), with variations in backazimuth estimates increasing the most. EROC analysis is divided into the first and second two-hours of data as a result of the changing noise conditions. During the first two-hours, PMCC produces higher detection probabilities (0.40-0.78) than AFD (0.22-0.45). PMCC also produces a more conservative estimate of detection based on false alarm probabilities from 0.03 to 0.07 compared to false alarm probabilities for AFD from 0.01 to 0.11. PMCC had the highest detection probabilities using a consistency of 0.1 s, almost twice the value when using a consistency of 0.9 s. AFD produces higher detection probabilities with larger p-values, the detection probability with a p-value of 0.05 is twice that compared to estimates using a p-value of 0.01. Both detectors have high false-alarm probabilities.

PMCC conservatively detects infrasound signals while AFD detects signals during high noise environment, although these detections may be correlated with noise. In all cases the analysts picked a higher number of signals than either automated process, including detections under higher noise conditions. Both detectors have lower detection probabilities under high wind conditions with a maximum probability of 0.45, compared to that of 0.78 under low noise conditions. PMCC produced few-detections (conservative detection) during the time period of

higher noise. The detection probabilities from AFD for the higher p-values increased and were accompanied by more false alarms.

The two detection methods rely on signal correlation. AFD adapts to changing background noise conditions with the number of detections controlled by the *p*-value of the F-statistics with an increased number of false alarms for higher *p*-values (0.09). PMCC uses the cross-correlation technique with the progressive method applied to a sub-network in both the time and frequency domain. By increasing the acceptable consistency value (up to 0.9 s), the detection probability increases under low noise conditions but these tests suggest that PMCC conservatively detects signals under high noise conditions. Using small and large aperture arrays together as a sub-network rather than using small or large aperture arrays separately provided higher detection probabilities illustrating the strength of arrays with a variety of spatial scales..

Generally, the numbers of automatic and human detections are dependent on the RMS amplitudes which are strongly affected by wind velocity. The number of detections in all cases significantly increases for small average RMS amplitudes between 1.2 and 3.2 mPa.

Based on the comparison of automated detections from AFD and the analysts, the use of combined small and large aperture arrays is recommended rather than using either the small or large aperture arrays alone. For PMCC, a combination of both small and large aperture arrays for the sub-network also improves the detection probability.

This study motivates the exploration of these automated detectors using longer time periods of data as well as additional arrays in order to further explore the impact of noise and geographic environments on both optimization of the procedures as well as characterization of performance. Extension of similar analysis to regional networks of infrasound arrays will

provide the capability to assess network performance including signal association and subsequent location across the area covered by the network.

Finally a list of individual conclusions:

- Both automatic detectors produce a larger number of detections when either the combined small and large aperture arrays or all array elements are used relative to the cases where the small or large aperture arrays are used alone.
- Results combining the small and large aperture arrays for detection combine individual detections found using the small aperture arrays and large aperture arrays separately.
- The numbers of detections estimated by AFD are almost twice that estimated by PMCC with many of the additional detections from AFD occurring in the last two-hour time period of data when wind noise increases.
- In all cases, the number of analyst detections is significantly higher than those determined by either automated detector.
- In most all cases, analysts identify all events detected by the two automatic processes.
- In the case of the last two hours of data where the noise levels are higher, there are fewer automated detections and a reduced number of detections identified by the analysts.
- During the first two-hours of data, cases using either all array elements or small and large aperture arrays together have higher detection probabilities than those using small or large aperture arrays alone with both detectors.
- Both detection and false alarm rate increase when using the higher *p*-values and smaller consistency.
- Based on the EROC which takes analyst's result as the reference, detection probabilities was negatively impacted by noise level, with low noise conditions (average amplitude of

497	1.7 mPa) producing an average detection probability of ~40% and high noise conditions
498	(average amplitude of 2.9 mPa) having an average detection probability of ~23%.
499	• Generally, the numbers of automatic and human detections are dependent on the RMS
500	amplitude, which is correlated with wind velocity.
501	• The number of detections in all cases significantly is high for average RMS amplitudes
502	between 1.2 and 3.2 mPa and includes most all the signals detected by the automated
503	procedures.
504	
505	Data and Resources
506	
507	Infrasound data used in this study was collected by Southern Methodist University (SMU) and
508	Korea Institute of Geoscience and Mineral Resources (KIGAM), and data is available through
509	the authors by approved request.
510	
511	Acknowledgments
512	
513	We would like to thank Dr. Yves Cansi of Commissariat à l'Energie Atomique (CEA) and Dr. Il-
514	Young Che of Korea Institute of Geoscience and Mineral Sources (KIGAM) for helpful
515	comments for the initial assessment of PMCC. We also thank Dr. Alexis Le Pichon of CEA and
516	Dr. Maurice Charbit of Institut Telecom for their valuable comments towards the improvement
517	our manuscript. We thank Mason MacPhail (SMU) and Dr. Petru Negraru (ION geophysical) for
518	volunteering the analyst review work. This work was funded by

520	
521	
522	
523	
524	
525	
526	
527	
528	References
529	
530	Arrowsmith, S. J., C. Hayward, B. Stump, R. Burlac, IY. Che, and G. Singh (2008). Multi-
531	Array Detection, Association and Location of Infrasound and Seismo-Acoustic Events in
532	Utah, in Proceeding of the 2008 Monitoring Research Review: Ground-Based Nuclear
533	Explosion Monitoring Technologies, LA-UR-08-05261 2 844-852.
534	Arrowsmith, S. J., R. Whitaker, C. Katz, and C. Hayward (2009). The F-Detector Revisited: An
535	Improved Strategy for Signal Detection at Seismic and Infrasound Arrays, Bull. Seismo.
536	Soc. Am. <b>99</b> 449-453.
537	Blandford, R. R. (2002). Detection and Azimuth Estimation by Infrasonic Arrays as a Function
538	of Array Aperture and Signal Coherence, AFTAC-TR-02 10-13
539	Blandford, R. R. (1974). An automatic event detector at the Tonto Forest seismic observatory,
540	Geophysiscs <b>39</b> 633-643.

- Brown, D. J., R. Whitaker, B. L. N. Kennett, and C. Tarlowski (2008). Automatic infrasonic
- signal detection using the Hough transform, J. Geophys. Res. 113 D17105,
- 543 doi:10.1029/2008JD009822.
- 544 Cansi, Y. (1995). An automated seismic event processing for detection and location: the
- P.M.C.C. method, *Geophys. Res. Lett.* **22** 1021-1024.
- Cansi, Y., and A. Le Pichon (2009). Infrasound Event Detection Using the Progressive Multi-
- Channel Correlation Algorithm, in *Handbook of Signal Processing in Acoustics*, D.
- Havelock, S. Kuwano, and M. Vorländer (Editors), Springer, New York, p. 1425-1435.
- Coyne, J., and I. Henson (1995). Geotool Sourcebook: User's Manual, Teledyne Brown
- Engineering, Scientific Report No. 1 PL-TR-96-2021.
- 551 Campus, P., and D. R. Christie (2010). Worldwide Observations of Infrasonic Waves, in
- Infrasound Monitoring for Atmospheric Studies A. Le Pichon, E. Blanc and A.
- Hauchecorne (Editors), Springer, New York, 185-234.
- Christie, D. R., and P. Campus (2010). The IMS infrasound network: Design and establishment
- of infrasound stations, in *Infrasound Monitoring for Atmospheric Studies* A. Le Pichon, E.
- Blanc and A. Hauchecorne (Editors), Springer, New York, 29–75.
- Evers, L. G., and H. W. Haak (2001). Listening to sounds from an exploding meteor and oceanic
- waves, Geophys. Res. Lett. 28 41–44, doi:10.1029/2000GL011859.
- Freedman, H. W. (1966). The "little variable factor" a statistical discussion of the reading of
- seismograms, *Bull. Seismo. Soc. Am.* **56** 593-604.
- Garcés, M., Hansen, R. A., and Lindquist, K. G. (1998). Traveltimes for infrasonic waves
- propagating in a stratified atmosphere, *Geophys. J. Int.* **135** 255-263.

563 Garcés, M., and C. Hetzer (2002). Evaluation of Infrasonic Detection Algorithms, in *Proceeding* of the 24th Seismic Research Review - Nuclear Explosion Monitoring: Innovation and 564 Integration, LA-UR-02-5048 2 745-754. 565 Hagerty, M. T., W.-Y. Kim, and P. Martysevich (1999). Characteristics of infrasound produced 566 by large mining explosions in Kazakstan, in *Proceedubg of the 21st Annual Seismic* 567 Research Symposium on Monitoring A Comprehensive Nuclear-Test-Ban Treaty 123-132. 568 Hart, D. (2004). Automated Infrasound Signal Detection Algorithms Implemented In MatSeis – 569 Infra Tool, Sandia Report SAND2004-1889. 570 Hedlin, M. A. H., C. de Groot-Hedlin, and D. Drob (2012). A study of Infrasound Propagation 571 Using Dense Seismic Network Recordings of Surface Explosions, Bull. Seismo. Soc. Am. 572 **102** 1927-1937, doi: 10.1785/0120110300. 573 574 Hough, P. V. C. (1959). Machine analysis of bubble chamber pictures, *Proc. Int. Conf. High* Energy Accelerators and Instrumentation. 575 Johnson, D. H., and D. E. Dudgeon (1993). Array Signal Processing: Concepts and Techniques, 576 577 Prentice Hall, Englewood Cliffs, New Jersey, 213-215. Kay S. (1998). Fundamentals of Statistical Signal Processing: Detection Theory, Volume II, 578 Prentice Hall, Englewood Cliffs, New Jersey, chap 3. 579 Leonard, M. (2000). Comparison of manual and automatic onset time picking, Bull. Seismo. Soc. 580 *Am.* **90** 1384-1390. 581

26

Matoza, R. S., M. Landès, A. Le Pichon, L. Ceranna, and D. Brown (2013). Coherent ambient

infrasound recorded by the International Monitoring System, Geophys. Res. Lett. 40

582

583

584

doi:10.1029/2012GL054329.

- Park, J., B. W. Stump, C. T. Hayward, S. J. Arrowsmith, and I.-Y. Che (2011). Multiple-Array
- Detection, Association, and Location of Infrasound and Seismo-Acoustic Event -
- Utilization of Ground Truth Information, in *Proceeding of the 2011 Monitoring Research*
- Review: Ground-Based Nuclear Explosion Monitoring Technologies 2 798-807.
- Park, J. (2013). Infrasound Signal Processing from Regional Arrays and Seismic Characteristics
- of North Korean Nuclear Explosions, Ph.D. Thesis, Southern Methodist University,
- 591 Dallas, TX, 27-36.
- Rost, S., and C. Thomas (2002). Array seismology: methods and applications, Rev. Geophys. 40
- 593 doi:10.1029/2000RG000100.
- Sereno, T. J. (1990). Attenuation of Regional Phases in Fennoscandia, and Estimates of Arrival
- Time and Azimuth Uncertainty using Data Recorded by Regional Arrays, SAIC-90/1472,
- Science Applications International Corp., San Diego, California.
- 597 Sipkin, S. A., W. J. Person, and B. W. Presgrave (2000). Earthquake bulletins and catalogs at the
- 598 USGS National Earthquake Information Center, in *Incorporate Research Institutions for*
- 599 Seismology Newsletter 2000 1 2-4.
- 600 Shumway, R. H., S. Kim, and R. R. Blandford (1999). Nonlinear estimation for time series
- observed on arrays, In Asymptotics, Nonparametrics, and Time Series S. Ghosh (Editor),
- Marcel Dekker, New York, 227-258.
- Vernon, F., J. Tytell, B. Busby, J. Eakins, M. Hedlin, A. Muschinski, K. Walker and B.
- Woodward (2012). Scientific Viability of the USArray Transportable Array Network As
- a Real-Time Weather Monitoring Platform, 92nd American Meteorological Society
- Annual Meeting (24 January 2012), New Orleans, LA.

507	Zeiler, C. P., and A. A. Velasco (2009). Seismogram Picking Error from Analyst Review
508	(SPEAR): Single-Analyst and Institution Analysis, Bull. Seismo. Soc. Am. 99 2759-2770.
509	
510	
511	
512	
513	
514	
515	
516	
517	
518	
519	
520	Full mailing address for each author
521	
522	Roy M. Huffington Department of Earth Sciences
523	Southern Methodist University
524	3225 Daniel Avenue
525	Dallas, TX75205, USA
526	(J.P., C.T.H, & B.W.S)
527	
528	Air Force Technical Application Center/TTRE,
529	Patrick AFB, FL, USA

630 (C.P.Z.)

632 Sandia National Laboratories,

633 1515 Eubank Blvd, Albuquerque, 87123, USA

634 (S.J.A.)

# Table 1

Parameters	Automatic detectors		
rarameters	AFD	PMCC	
Filter band (Hz)	1-5		
Time window (s)	20		
Overlap (%)	50		
<i>p</i> -value	0.01 & 0.05	-	
Adaptive window (h)	1	-	
Consistency (s)	=	0.1 & 0.5	

Detection processing parameters

Detection processing parameters used in initial tests of automatic detectors, AFD and PMCC.

Table 2

Configurations of CHNAR used in this study

Configurations	Aperture size	Arrays used for test
AFD(S)/PMCC(S)	A small aperture (<100m) array	CHN00/03/04/05
AFD(L)/PMCC(L)	A large aperture (~1km) array	CHN00/10/20/30
AFD(S+L)	A hybrid of small and large	CHN00/03/04/05/10/20/30
PMCC(S+L)	aperture arrays	Sub-network(CHN00/03/04/05)
TWICC(S+L)	aperture arrays	+Sub-network(CHN00/10/20/30)
AFD(All)		CHN00/03/04/05/10/20/30/12/22/32
	A combination of small, large,	Sub-network(CHN00/03/04/05)
PMCC(All)	and sub-large aperture arrays	+Sub-network(CHN00/10/20/30)
		+Sub-network(CHN02/12/22/32)

Four different starting configurations of CHNAR for testing of PMCC and AFD.

Table 3

The numbers of detections estimated by AFD and PMCC.

Configuration	The numbers of detections	Configuration	The numbers of detections
AFD.01 (S)	52	PMCC.1s (S)	21
AFD.01 (L)	15	PMCC.1s (L)	8
AFD.01 (S+L)	39	PMCC.1s (S+L)	22
AFD.01 (All)	53	PMCC.1s (All)	22
AFD.05 (S)	65	PMCC.5s (S)	21
AFD.05 (L)	21	PMCC.5s (L)	11
AFD.05 (S+L)	59	PMCC.5s (S+L)	21
AFD.05 (All)	81	PMCC.5s (All)	26

The numbers of detections estimated by AFD and PMCC using the four different starting configurations (Table 2) with different detection thresholds (*p*-values of 0.01 and 0.05 for AFD, and consistency values of 0.1 s and 0.5 s for PMCC).

Table 4Analysts defined bandwidth for data review.

Ī		Analyst 1	Analyst 2	Analyst 3	Analyst 4	Analyst 5
	Filter band (Hz)	1.0-5.0	1.0-5.0	0.5-4.0	1.0-5.0	4.0-8.0

The bandwidth used by five analysts for data review in this study.

Figure 1. The physical configuration of CHNAR. The four-elements in the 1-km aperture seismo-acoustic array, CHN00/10/20/30 (circles) each have a GS-13 seismometer and infrasound gauge (Chaparral Physics Model 2.0) supplemented by a small aperture (< 100 m) infrasound subarray, CHN00/03/04/05 (squares) deployed around the center element. Each of three outer sites has an additional infrasound gauge, CHN12/22/32 (triangles), offset by about 50 m from the primary while the additional infrasound gauge, CHN02 is colocated with CHN00. 

Figure 2. The four-hour-dataset (02:00:00-06:00:00 in UTC, 11am-3pm in local time, Julian day 002, 2012) recorded at the seismo-acoustic array, CHNAR. Waveforms were filtered from 1 to 5 Hz.

733 velocity and azimuth) for the different array apertures used in detector testing during the four-hour-dataset at CHNAR (02:00:00-06:00:00 in UTC, Julian day 002, 2012) in the 734 735 above. Figure 4. Summary of detection results from PMCC.1s (All) with a consistency of 0.1 s using all 736 arrays (number of sensors, consistency, correlation, amplitude, azimuth, and phase 737 738 velocity). The waveform beam is displayed at the top with an example filtered waveform (CHN00) below. 739 Figure 5. The detection results from the two automatic detectors (PMCC and AFD) using 740 different sub-arrays (S: small aperture arrays, L: large aperture arrays, S+L: small and 741 large aperture arrays, and All: all arrays). (a) The result for the case with a maximum 742 743 consistency of 0.1 s for PMCC (PMCC.1s) and p-value of 0.01 for AFD (AFD.01). (b) The result for the case with a maximum consistency of 0.5 s for PMCC (PMCC.5s) and 744 p-value of 0.05 for AFD (AFD.05). The correlation values for detection are represented 745 746 by the colors in the plot with the azimuthal distribution of detections plotted to the far right. 747 Figure 6. Comparison of the total number of analyst and automatic picks (AFD.01: p-value, 0.01, 748 AFD.05: p-value, 0.05, PMCC.1s: consistency, 0.1 s, and PMCC.5s: consistency, 0.5 s) 749 for the four-hour block of infrasound data recorded at CHNAR. 750 Figure 7. Detection times from the automatic detectors (PMCC: PMCC.1s (Consistency, 0.1 s), 751 and PMCC.5s (Consistency, 0.5 s) and AFD: AFD.01 (p=0.01) and AFD.05 (p=0.05)) 752

Figure 3. The relationship between C value from AFD and wind conditions (average wind

732

753

and those estimated by the five analysts.

Figure 8. The azimuth and phase velocity estimates from the automatic detectors (PMCC.1s and PMCC.5s results, red and pink open circles and AFD.01 and AFD.05 results, blue and sky-blue open circles) and the analyst review (same color designation as in Figure 8).

754

755

756

774

775

- Figure 9. Polar plot of azimuth and phase velocity estimates from the analysts (left) and the automatic detectors (right) for the first two-hours of data (top) and the last two-hours of data (bottom).
- Figure 10. The *Estimated* Receiver Operating Characteristic (*E*ROC) for the automatic detectors using the first two-hours of data and different aperture arrays. For AFD, *p*-values of 0.01 (red circle), 0.03 (yellow circle), 0.05 (sky-blue circle), 0.07 (green circle), and 0.09 (gray circle) were used for the tests. For PMCC, consistency values of 0.1 s (red circle), 0.3 s (yellow circle), 0.5 s (skyblue circle), 0.7 s (green circle), and 0.9 s (gray circle) were used for the tests. The x-axes, False-alarm Probability, are exaggerated by a factor of seven.
- Figure 11. The *Estimated* Receiver Operating Characteristic (*E*ROC) for the automatic detectors using the second two-hours of data and different aperture arrays. For AFD, *p*-values of 0.01 (red circle), 0.03 (yellow circle), 0.05 (sky-blue circle), 0.07 (green circle), and 0.09 (gray circle) were used for the tests. For PMCC, consistency values of 0.1 s (red circle), 0.3 s (yellow circle), 0.5 s (skyblue circle), 0.7 s (green circle), and 0.9 s (gray circle) were used for the tests. The x-axes, False-alarm Probability, are exaggerated by a factor of three.
  - Figure 12. Top The average RMS amplitude (green line) as a function of time estimated using all waveforms compared to the amplitude (left y-axis) and duration (colorbar) of the detected signals identified by Analyst 5. Bottom The wind velocity recorded at CHNAR

during the four-hour time period plotted as a function of time. Superimposed on this plot is the average wind velocity for five-minute windows with standard deviation (sky-blue vertical bar) and average wind direction (colorbar), which can be compared to amplitude data in the top plot.

Figure 13. The relationship between the number of detections estimated by (a) the automated analysis and (b) the analyst review during five-minute windows compared to wind velocity and average RMS amplitude (mPa) for each window.

Figure 14. The cumulative number of detections in all the five-minute windows for both the automatic detectors and the analyst plotted against (a) the average RMS amplitude (mPa) in the window and (b) against 1/(average RMS amplitude) which is proportional to the signal to noise ratio (SNR).

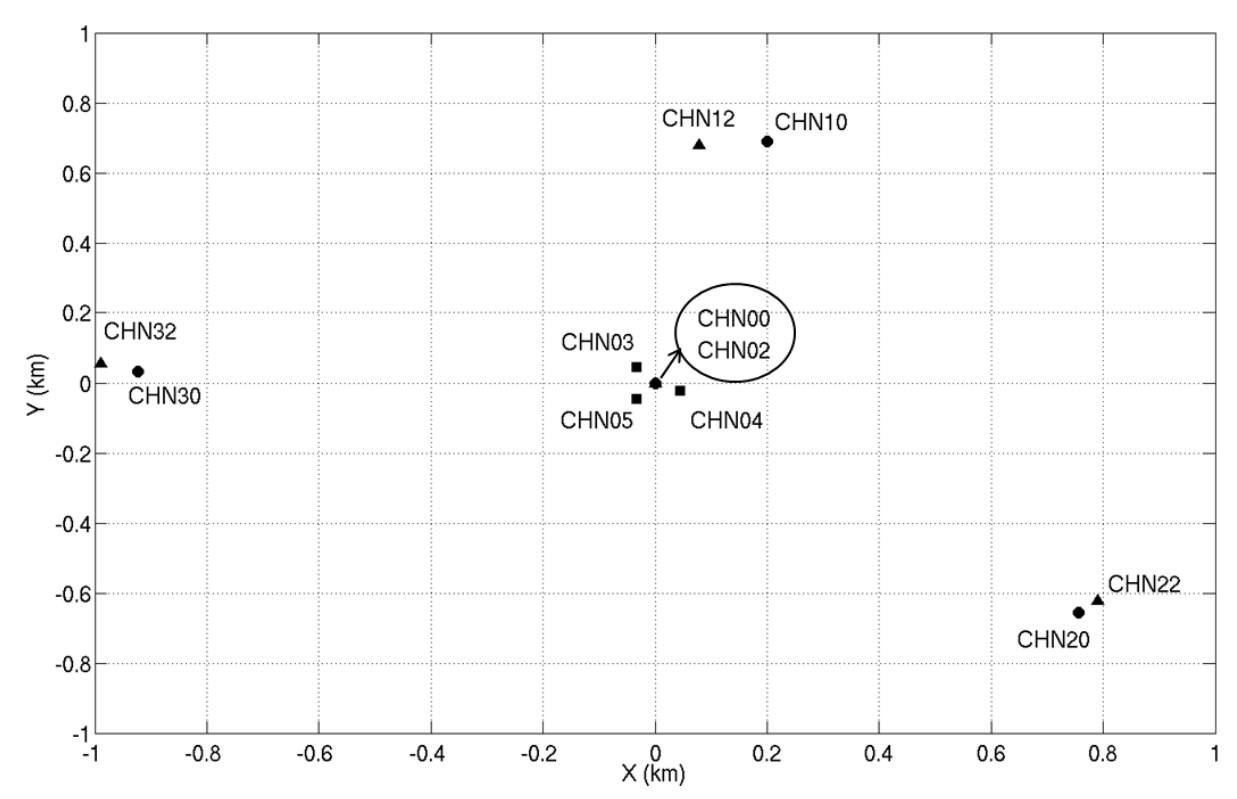


Figure 1. The physical configuration of CHNAR. The four-elements in the 1-km aperture seismo-acoustic array, CHN00/10/20/30 (circles) each have a GS-13 seismometer and

infrasound gauge (Chaparral Physics Model 2.0) supplemented by a small aperture (< 100 m) infrasound subarray, CHN00/03/04/05 (squares) deployed around the center element. Each of three outer sites has an additional infrasound gauge, CHN12/22/32 (triangles), offset by about 50 m from the primary while the additional infrasound gauge, CHN02 is colocated with CHN00.

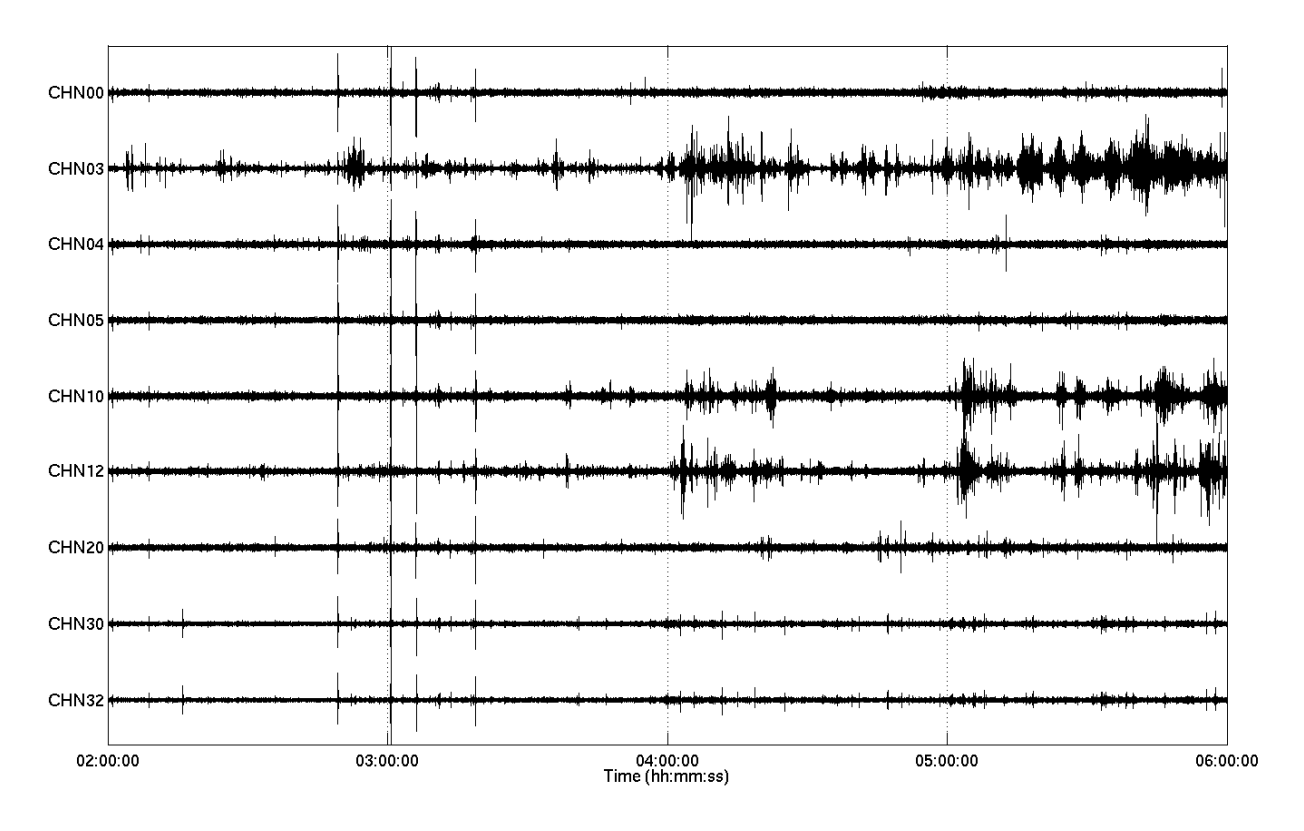


Figure 2. The four-hour-dataset (02:00:00-06:00:00 in UTC, 11am-3pm in local time, Julian day 002, 2012) recorded at the seismo-acoustic array, CHNAR. Waveforms were filtered from 1 to 5 Hz.

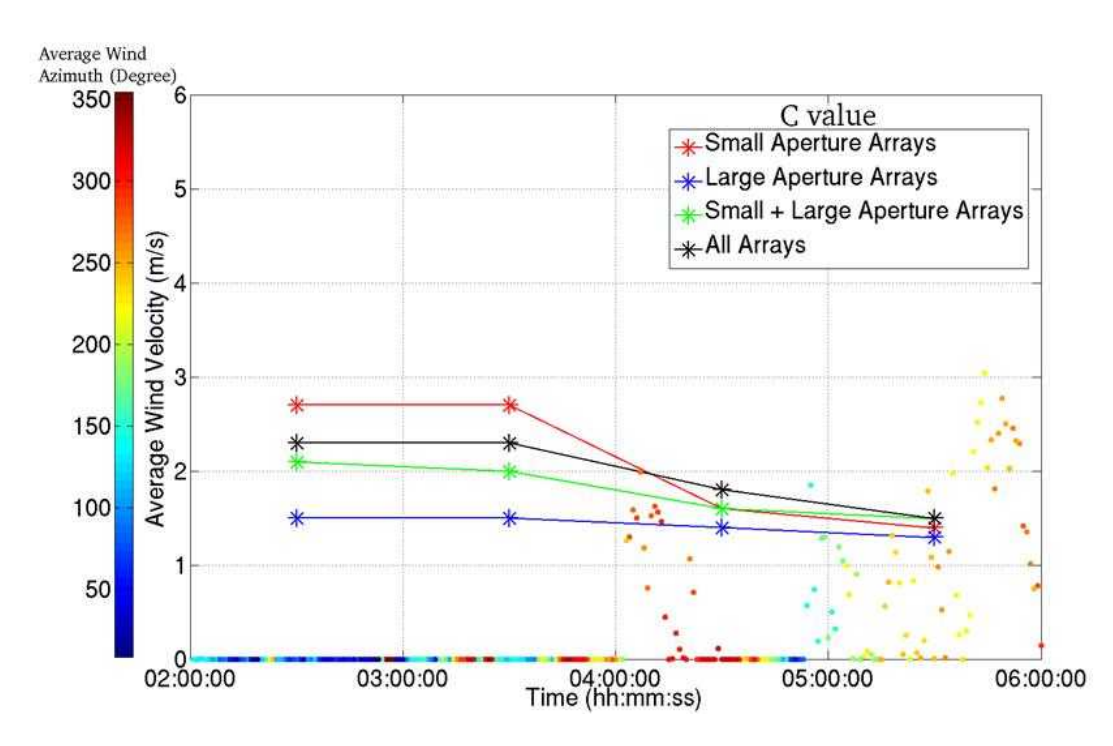


Figure 3. The relationship between C value from AFD and wind conditions (average wind velocity and azimuth) for the different array apertures used in detector testing during the four-hour-dataset at CHNAR (02:00:00-06:00:00 in UTC, Julian day 002, 2012) in the above.

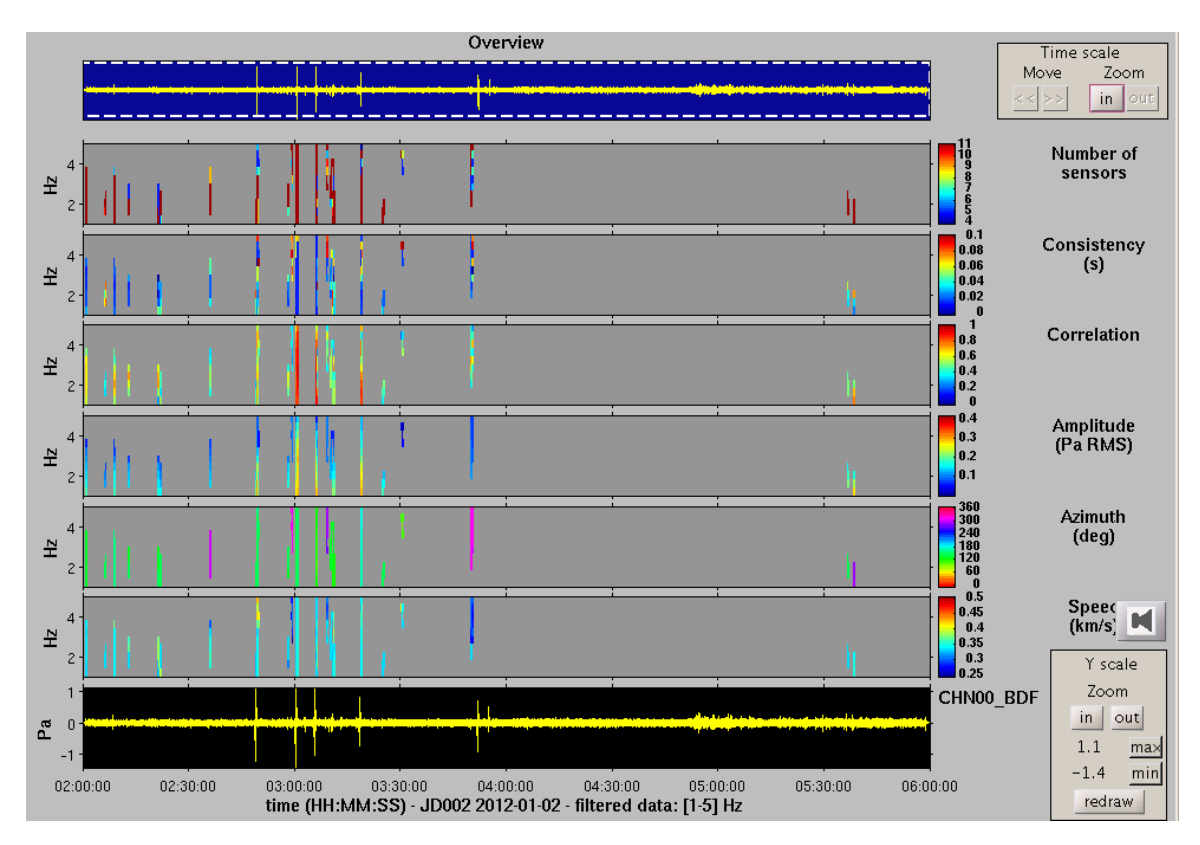


Figure 4. Summary of detection results from PMCC.1s (All) with a consistency of 0.1 s using all arrays (number of sensors, consistency, correlation, amplitude, azimuth, and phase velocity). The waveform beam is displayed at the top with an example filtered waveform (CHN00) below.

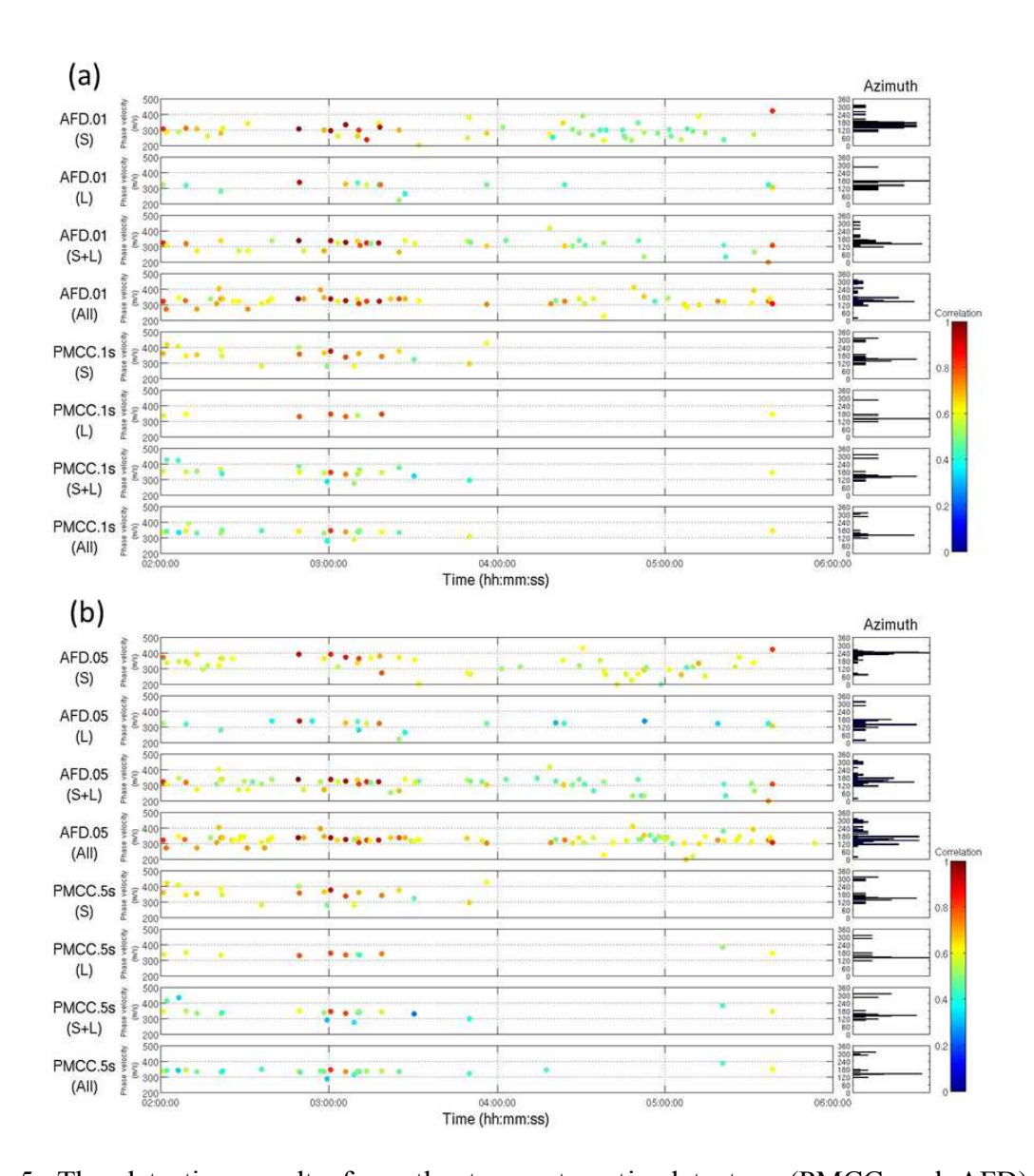


Figure 5. The detection results from the two automatic detectors (PMCC and AFD) using different sub-arrays (S: small aperture arrays, L: large aperture arrays, S+L: small and large aperture arrays, and All: all arrays). (a) The result for the case with a maximum consistency of 0.1 s for PMCC (PMCC.1s) and *p*-value of 0.01 for AFD (AFD.01). (b) The result for the case with a maximum consistency of 0.5 s for PMCC (PMCC.5s) and *p*-value of 0.05 for AFD (AFD.05). The correlation values for detection are represented by the colors in the plot with the azimuthal distribution of detections plotted to the far right.

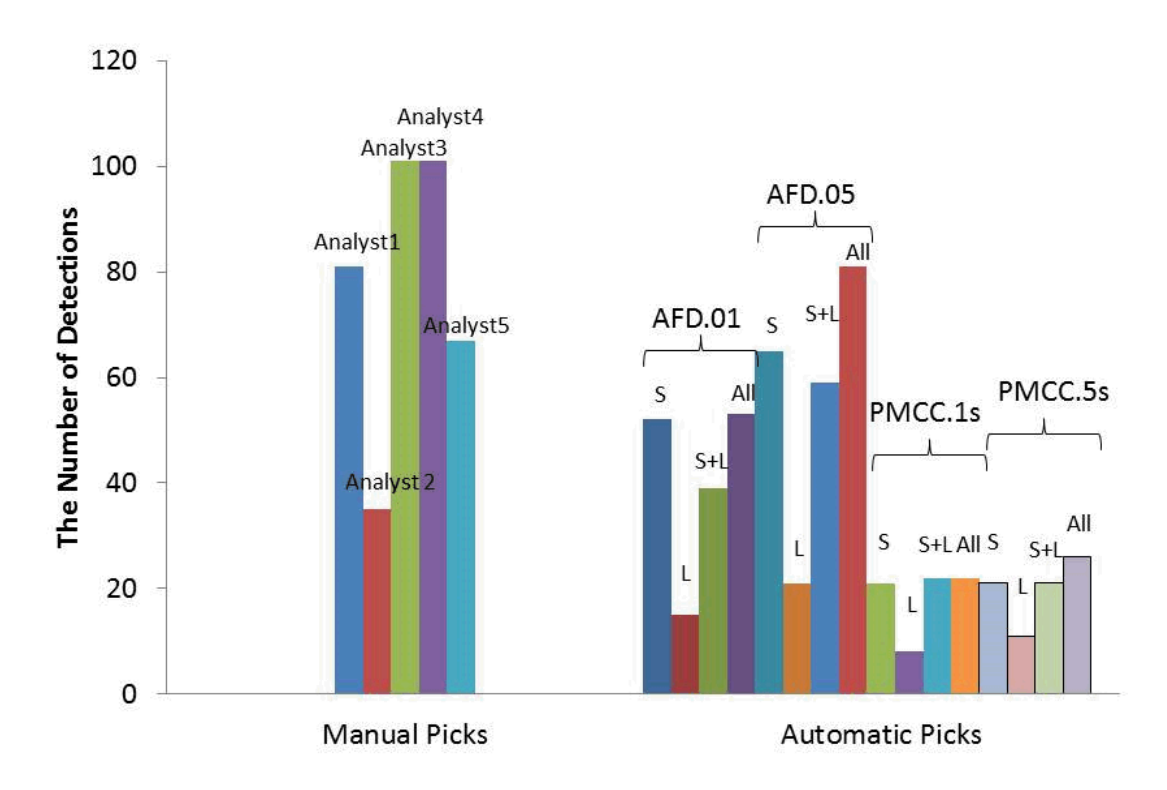


Figure 6. Comparison of the total number of analyst and automatic picks (AFD.01: *p*-value, 0.01, AFD.05: *p*-value, 0.05, PMCC.1s: consistency, 0.1 s, and PMCC.5s: consistency, 0.5 s) for the four-hour block of infrasound data recorded at CHNAR.

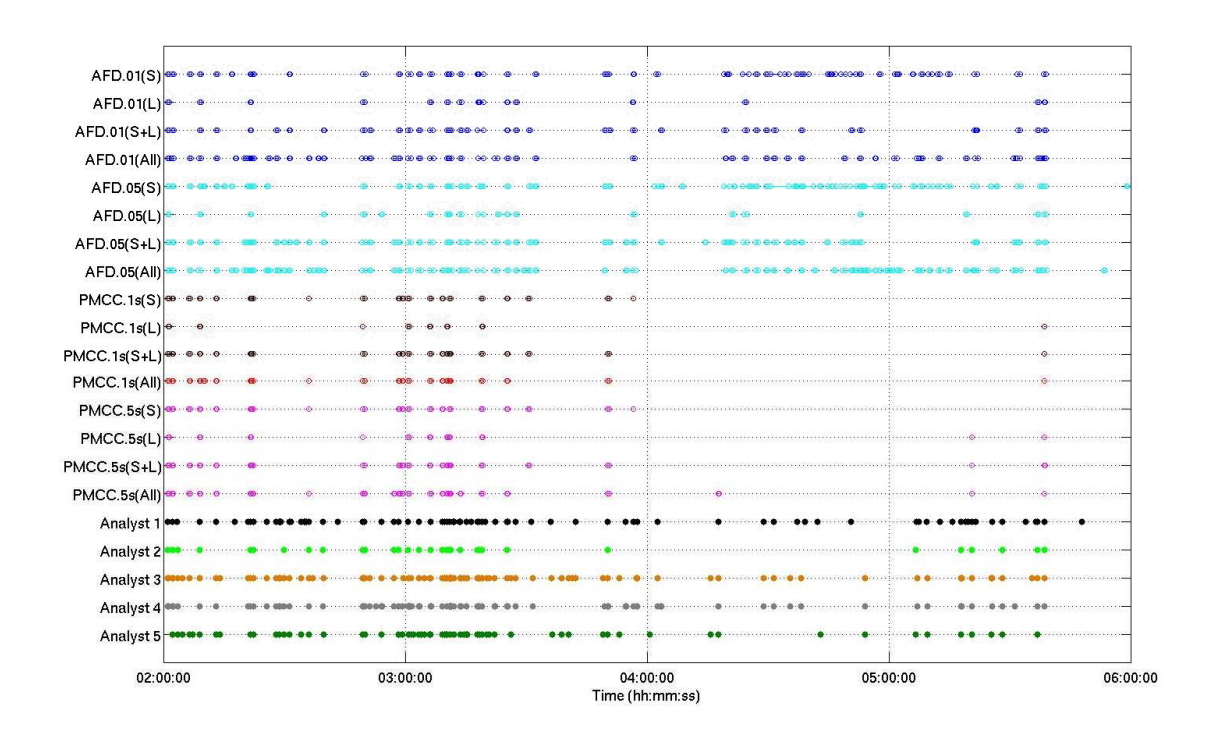


Figure 7. Detection times from the automatic detectors (PMCC: PMCC.1s (Consistency, 0.1 s), and PMCC.5s (Consistency, 0.5 s) and AFD: AFD.01 (p=0.01) and AFD.05 (p=0.05)) and those estimated by the five analysts.

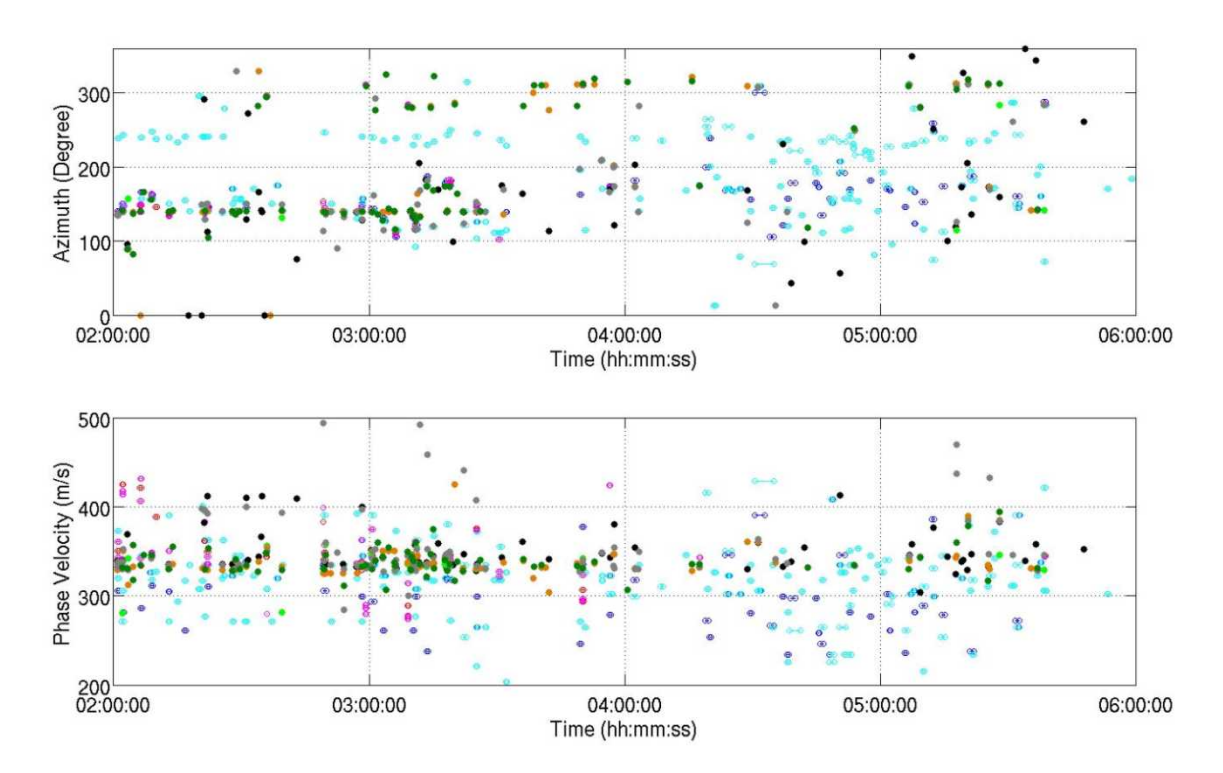


Figure 8. The azimuth and phase velocity estimates from the automatic detectors (PMCC.1s and PMCC.5s results, red and pink open circles and AFD.01 and AFD.05 results, blue and sky-blue open circles) and the analyst review (same color designation as in Figure 8).

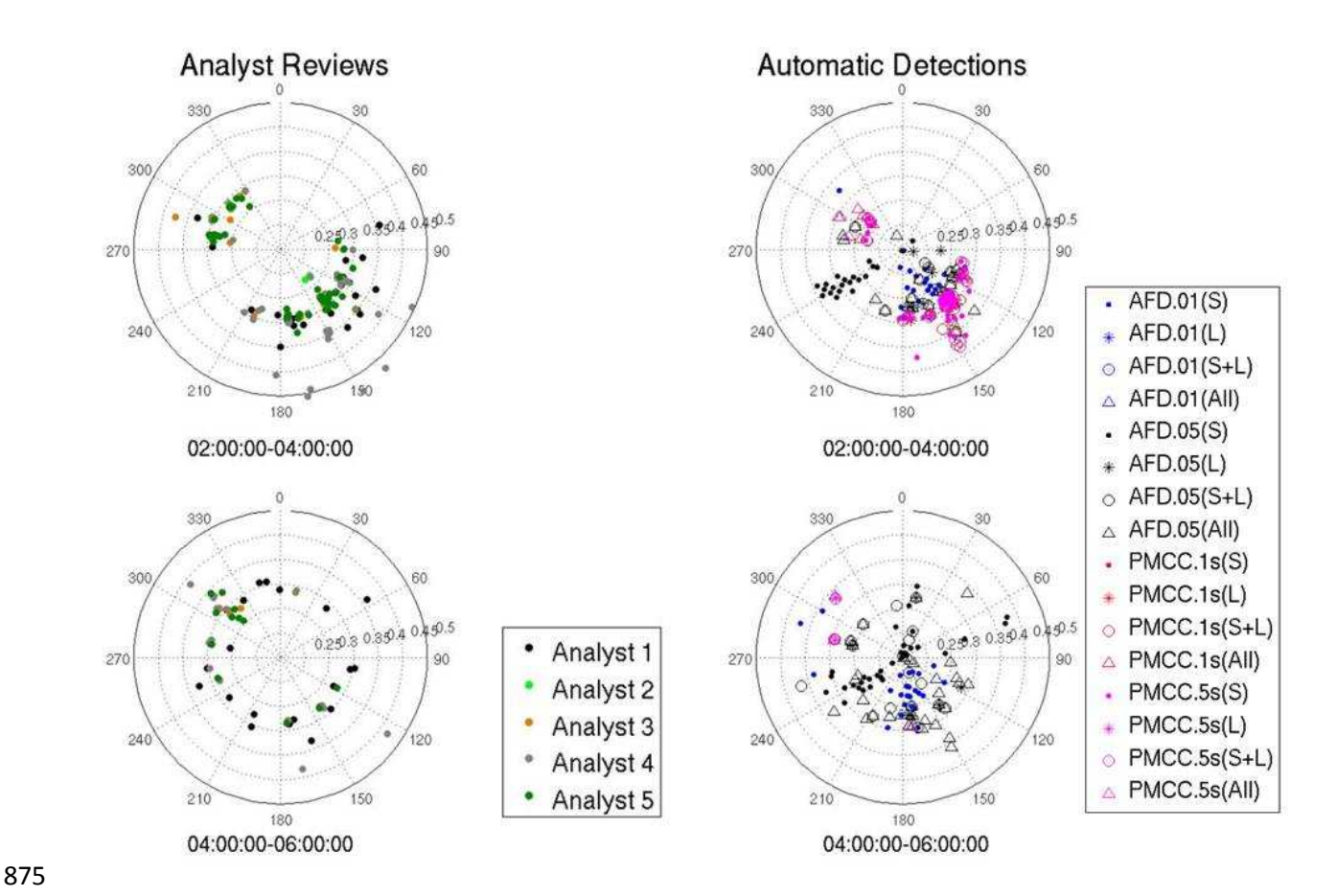


Figure 9. Polar plot of azimuth and phase velocity estimates from the analysts (left) and the automatic detectors (right) for the first two-hours of data (top) and the last two-hours of data (bottom).

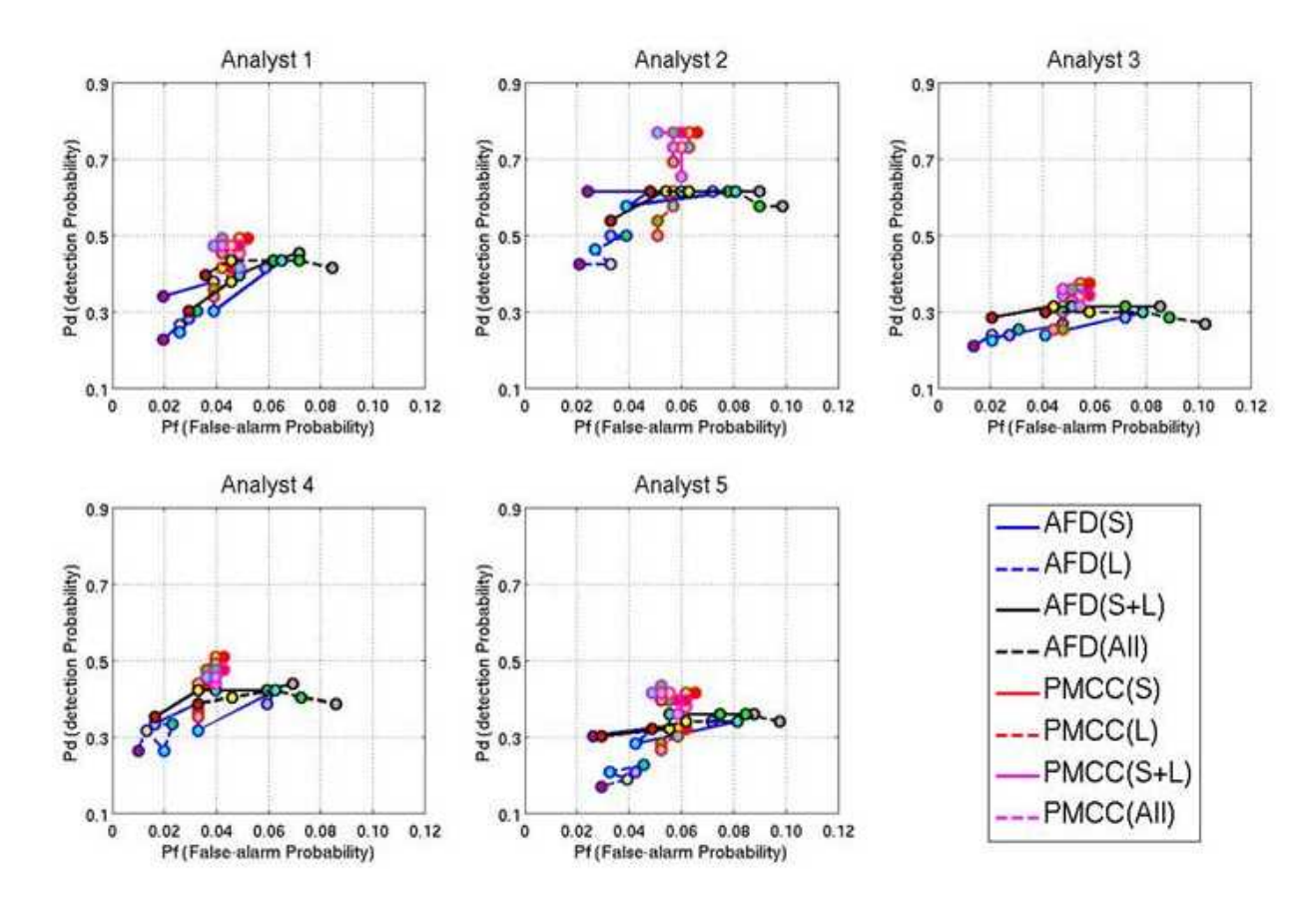


Figure 10. The *Estimated* Receiver Operating Characteristic (*E*ROC) for the automatic detectors using the first two-hours of data and different aperture arrays. For AFD, *p*-values of 0.01 (red circle), 0.03 (yellow circle), 0.05 (sky-blue circle), 0.07 (green circle), and 0.09 (gray circle) were used for the tests. For PMCC, consistency values of 0.1 s (red circle), 0.3 s (yellow circle), 0.5 s (skyblue circle), 0.7 s (green circle), and 0.9 s (gray circle) were used for the tests. The x-axes, False-alarm Probability, are exaggerated by a factor of seven.

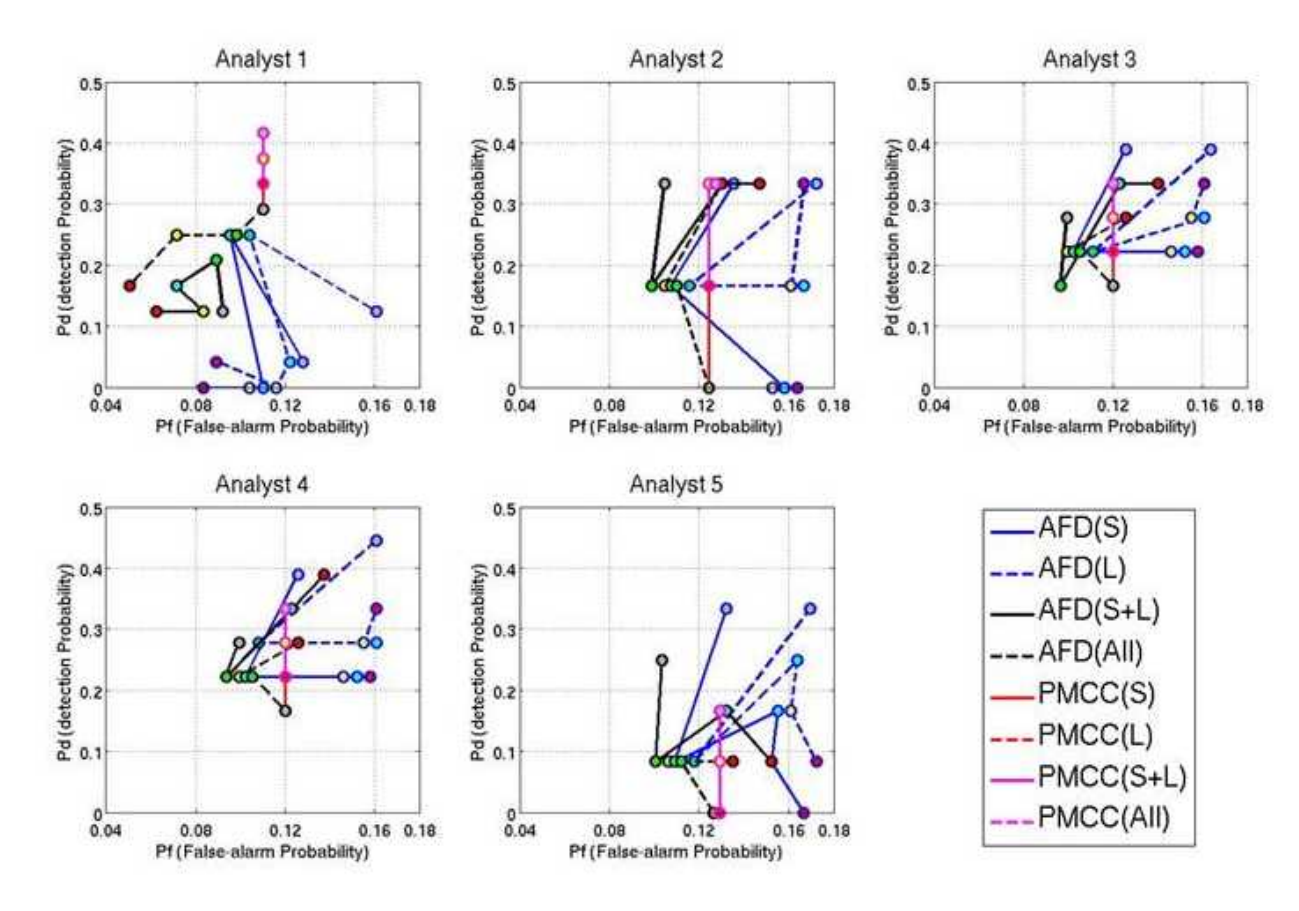


Figure 11. The *Estimated* Receiver Operating Characteristic (*E*ROC) for the automatic detectors using the second two-hours of data and different aperture arrays. For AFD, *p*-values of 0.01 (red circle), 0.03 (yellow circle), 0.05 (sky-blue circle), 0.07 (green circle), and 0.09 (gray circle) were used for the tests. For PMCC, consistency values of 0.1 s (red circle), 0.3 s (yellow circle), 0.5 s (skyblue circle), 0.7 s (green circle), and 0.9 s (gray circle) were used for the tests. The x-axes, False-alarm Probability, are exaggerated by a factor of three.

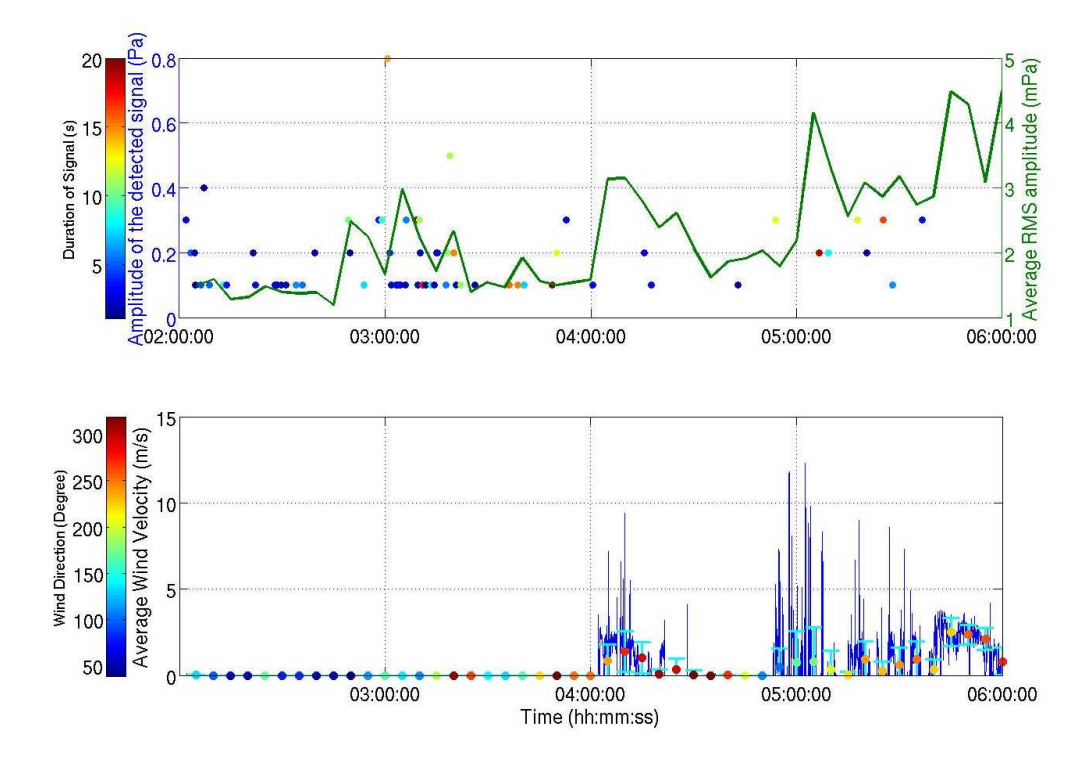


Figure 12. Top - The average RMS amplitude (green line) as a function of time estimated using all waveforms compared to the amplitude (left y-axis) and duration (colorbar) of the detected signals identified by Analyst 5. Bottom - The wind velocity recorded at CHNAR during the four-hour time period plotted as a function of time. Superimposed on this plot is the average wind velocity for five-minute windows with standard deviation (sky-blue vertical bar) and average wind direction (colorbar), which can be compared to amplitude data in the top plot.

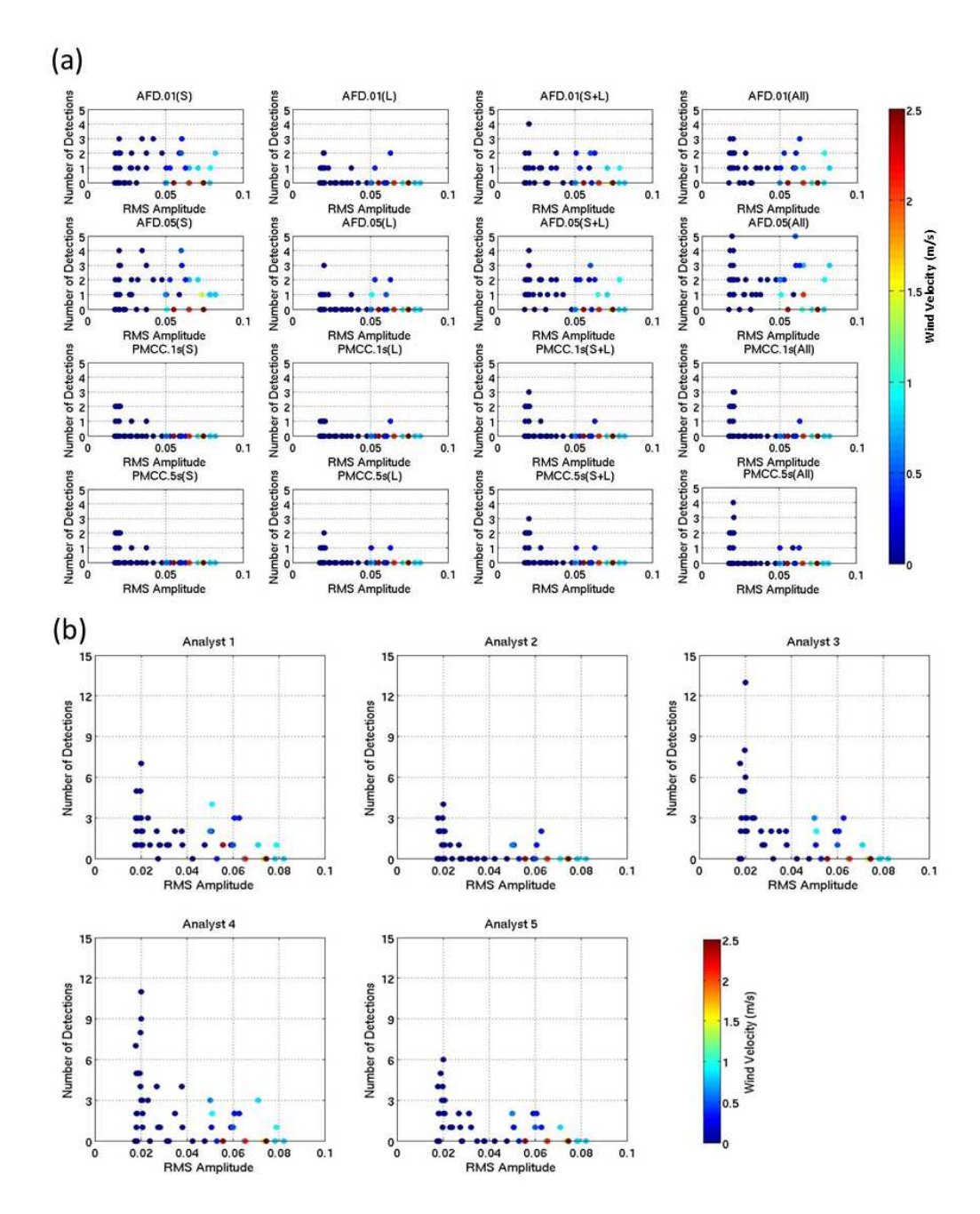


Figure 13. The relationship between the number of detections estimated by (a) the automated analysis and (b) the analyst review during five-minute windows compared to wind velocity and average RMS amplitude (mPa) for each window.

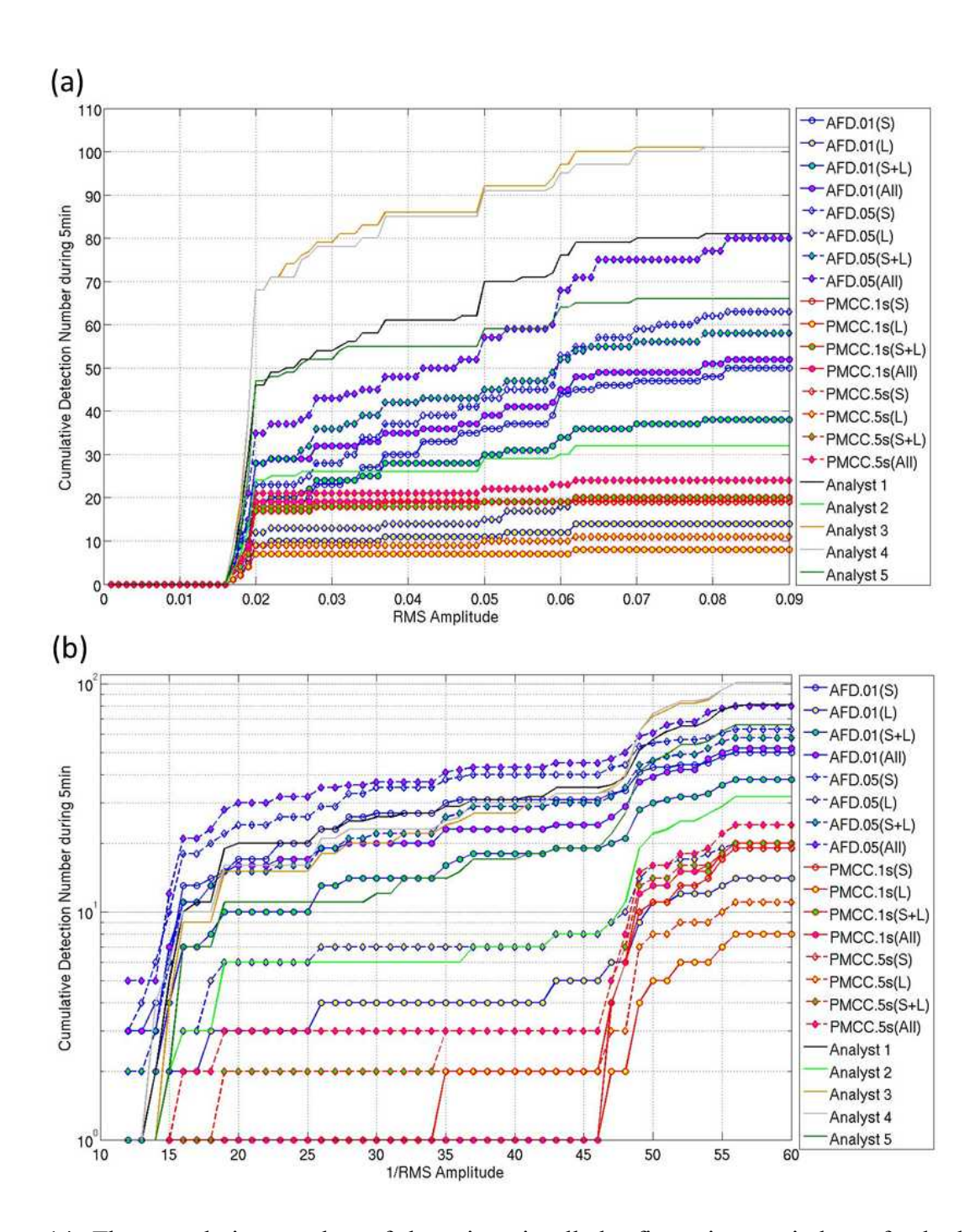


Figure 14. The cumulative number of detections in all the five-minute windows for both the automatic detectors and the analyst plotted against (a) the average RMS amplitude (mPa) in the window and (b) against 1/(average RMS amplitude) which is proportional to the signal to noise ratio (SNR).